

## RESTORATION OF SHADOW DETAILS IN PROJECTED FRINGE PROFILOMETER IMAGES

K.G.Larkin, P.S.Fairman, D.I.Farrant, and B.F.Oreb  
CSIRO Division of Applied Physics, Lindfield, NSW

### ABSTRACT

A technique for deriving the translation, rotation, and scaling differences of two related digital images has been developed for a 3-D measurement instrument. Because of restricted illumination and viewing angles there are, in general, some obscured image regions. By combining images from two views - which must be accurately registered - a single image with no obscurations can be produced. The mathematical principles of the process - known as *phase-only correlation* - are outlined and various steps in the process are illustrated with computed images. The correspondence of processing in the real space domain and the Fourier space domain is demonstrated. Typical accuracies of  $\pm 0.3$  pixel over a range of  $\pm 20$  pixels are obtained. Some improvements to the technique for increased accuracy are identified.

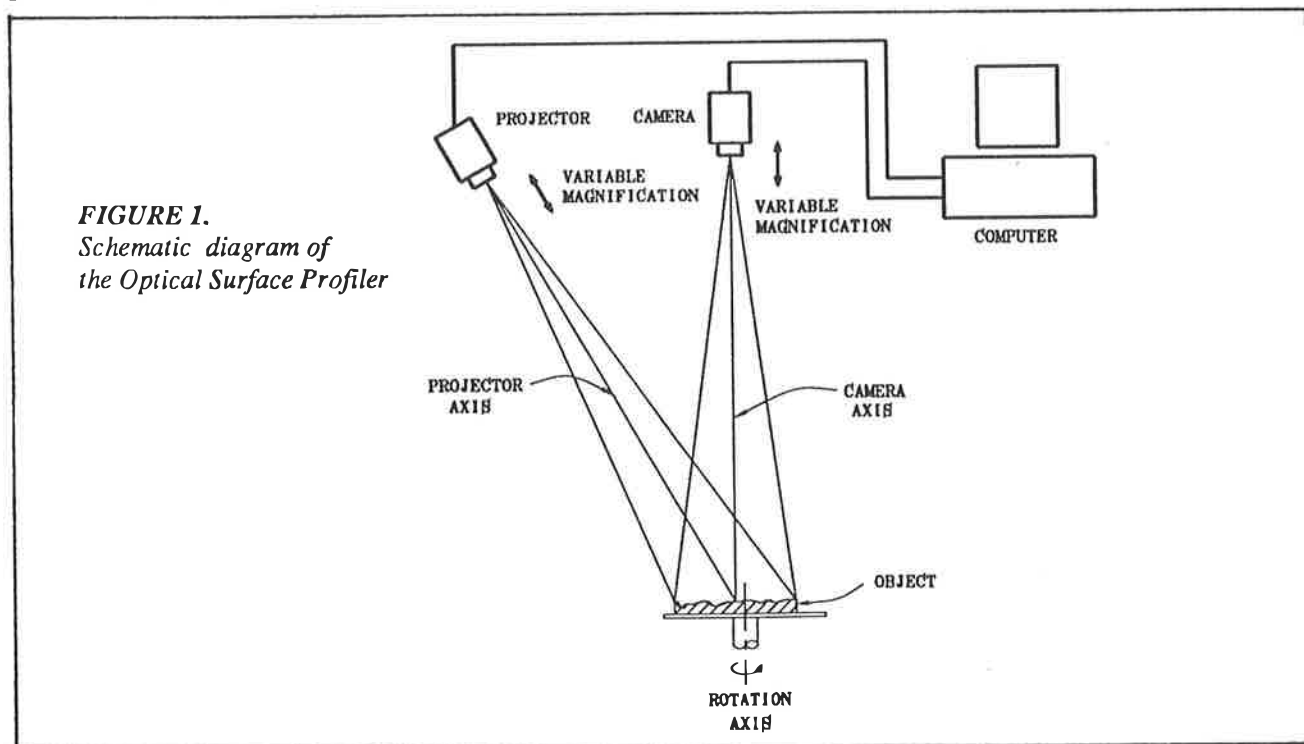
### INTRODUCTION

Accurate shape measurement is an important part of many manufacturing processes. The CSIRO Division of Applied Physics has developed a number of optical systems for non-contact shape measurement. One instrument we have recently developed is the Optical Surface Profiler (OSP130) which is used for the non-contact metrology of master tooling at the Royal Australian Mint. Tooling with diameters in the range 10mm to 300mm can be measured over a large array of equally spaced points, typically 560x560. This instrument uses a technique called projected fringe profilometry which will be explained in the next section. Until recently a major limitation of the technique has been the maximum slope of surface features which could be measured due to shadowing effects resulting from the finite projection angle.

### INTRODUCTION TO PROJECTED FRINGE PROFILOMETRY

Projected fringe profilometry is an optical, non-contact technique for measuring surface topography. In essence a fringe pattern is projected onto an object and the distorted fringe pattern viewed by a camera from a different direction. The distortion is related to the height variation of the object. High accuracy can be achieved if the exact phase of the distorted fringe is known. Using a technique known as phase stepping interferometry it is possible to determine precisely the phase of a fringe from a minimum of three measurements of fringe intensity. Further details of the technique can be found in [1] and [2].

Figure 1 is a schematic diagram of the OSP. A white light projector forms the image of a sinusoidal grating upon the surface of the object to be measured. A TV camera placed directly above the object views the deformed light pattern. The grating is shifted, in-plane, to a number of well defined locations under the control of the computer.



At each location a TV image of the irradiance pattern is digitized and stored by a frame grabber inside the computer. A simple algorithm is then used to calculate the phase of the deformed sinusoid at every point in the array. The calculated phase is directly related to the object surface height by a geometric factor which varies in a well defined manner across the surface.

Consider figure 2. The reflected light imaged by the camera at any point (x,y) on the object surface, can be expressed as I, where:

$$I(x,y) = R(x,y) \cdot I_0(x,y) \cdot \{ 1 + A \cdot \cos(2\pi[x + z \cdot \tan(\beta)] / \lambda_s) \} \quad (1)$$

and:  $R(x,y)$  is the surface reflectance at any point,  $I_0(x,y)$  is the irradiance,  
 $A$  is the fringe modulation,  $z = z(x,y)$  is the object height,  
 $\lambda_s$  is the undistorted fringe period, and  $\beta$  is the projection angle from vertical.

For a collimated projection system both  $\beta$  and  $\lambda_s$  are constants. In a divergent system they are functions of x. The equation representing the light variation has three unknowns, ( $R \cdot I_0$ ),  $A$ , and  $z$ . The solution requires a minimum of three simultaneous equations. These are created by shifting the pattern a known amount so that there is a shift in the intensity at the surface. By doing this at least twice, we can create the set of simultaneous equations that we require. This introduced phase shift is the heart of phase stepping interferometry. Although three steps are sufficient for the determination of the fringe phase, it can be shown [3] that sensitivity to some errors can be substantially reduced by using five steps. In this case the corresponding expression for equation (1) at every point, (x,y), in the field is :

$$\begin{aligned} I_1 &= R \cdot I_0 ( 1 + A \cos( \varphi - 2\delta ) ) \\ I_2 &= R \cdot I_0 ( 1 + A \cos( \varphi - \delta ) ) \\ I_3 &= R \cdot I_0 ( 1 + A \cos( \varphi ) ) \\ I_4 &= R \cdot I_0 ( 1 + A \cos( \varphi + \delta ) ) \\ I_5 &= R \cdot I_0 ( 1 + A \cos( \varphi + 2\delta ) ) \end{aligned} \quad \begin{aligned} &\text{where } \delta \text{ is the introduced phase step.} \\ &\text{and } \varphi = 2\pi [ x + z \cdot \tan(\beta) ] / \lambda_s \end{aligned} \quad (2)$$

The phase can be calculated using the following relation when the phase step  $\delta = \pi/2$  :

$$\tan(\varphi) = 2 \cdot ( I_2 - I_4 ) / ( 2 \cdot I_3 - I_5 - I_1 ) \quad (3)$$

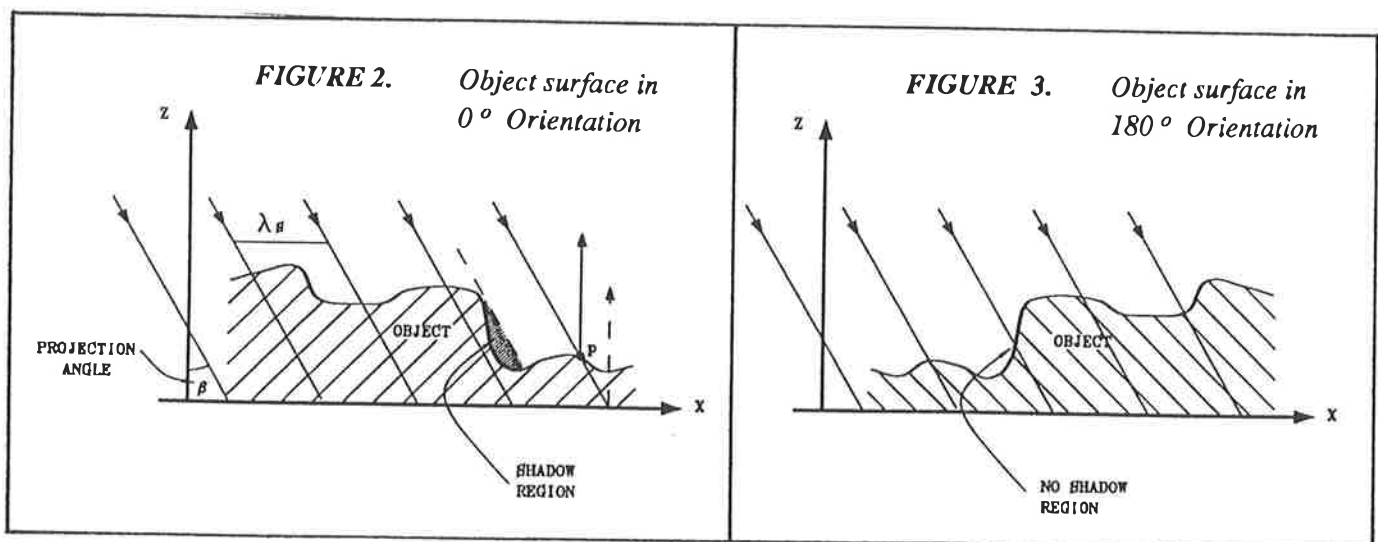
Generally  $\lambda_s$  is not known accurately before a measurement is performed. The system is calibrated by using a flat surface ( $z(x,y) = 0$ ) as a reference object. The phase of such an object is  $\varphi_0(x,y) = 2\pi \cdot x / \lambda_s$ . From this  $\lambda_s$  can be calculated. Placing the object to be measured in the system results in the object phase map  $\varphi_s(x,y)$  given by equation (2). The simplest method of deriving the the height distribution is as follows:

Calculate object and reference phase:  $\varphi_s(x,y)$ ,  $\varphi_0(x,y)$ . Calculate the fringe spacing  $\lambda_s = 2\pi \cdot x / \varphi_0(x,y)$ .  
 Subtract phase maps  $\varphi_d = \varphi_s - \varphi_0$  Calculate the height  $z = \varphi_d \cdot \lambda_s / \{ 2\pi \cdot \tan(\beta) \}$ . (4)

The geometric parameters of the system are chosen so that  $-\pi < \varphi_d < \pi$ . This ensures that any ambiguities resulting from the modulo  $2\pi$  calculation of equation (3) are avoided. Physically this means that the fringe distortion must be limited to +/- 1/2 a fringe from the reference fringe pattern.

### SHADOW DETECTION

Shadow regions can be detected just prior to evaluation of equation (3). Two methods are applicable: the first checks to ensure all five light levels,  $I_n$ , are above a threshold value; the second checks that the fringe modulation,  $A$ , is above yet another threshold. In either case if the value is below threshold a shadow is deemed present. The process is repeated for all points within the field.



## THE PRINCIPLE OF SHADOW RESTORATION

The surface to be profiled is illuminated by a beam at an angle  $\beta$  to the vertical. Figure 2 shows a profile of the surface in the  $0^\circ$  orientation. Note the shadow region. The measurement sensitivity is determined by  $\beta$  in equation (4) If any part of the surface has a slope angle of less than  $\beta$  to the vertical then it will cast a shadow in either one of the two measurement orientations ( $0^\circ$  or  $180^\circ$ ). Figure 3 shows a profile of the surface in the  $180^\circ$  orientation. Note that no shadows occur in this particular instance.

Coins and coin dies have generally well behaved surfaces: the surface profile function  $z = f(x,y)$  is single valued and typically does not have steep features which can cast overlapping shadows in both orientations. Consequently measurements made in the  $0^\circ$  orientation will have different shadow regions to measurements made in the  $180^\circ$  orientation. This means, in principle, that the shadow regions in one orientation can have the correct height values restored from data in the corresponding unshadowed regions of the other orientation. It is necessary to overlay the measurements from both orientations, and register them accurately, to obtain adequate restoration of shadow detail.

## TWO DIMENSIONAL IMAGE REGISTRATION

In a measurement system with high precision components and exact alignment it is possible to produce a  $180^\circ$  rotation about a precisely defined axis. In such a system it is only necessary to rotate the  $180^\circ$  image back through  $180^\circ$  in software to obtain two perfectly registered images for the shadow restoration process. However, the cost and instability of such a system is very unattractive in a commercial instrument. A system which could allow a certain misregistration and then correct for it precisely was sought. With commercially available components it is possible to keep the misregistration to less than 20 pixels. However, the current accuracy requirements for height resolution mean that the shadow regions must be replaced with an accuracy of better than  $1/2$  pixel. A review of four registration techniques [4] indicated that the phase-only correlation technique works for large misregistrations (in other words it is robust) and can have an accuracy of better than 0.1 pixel. The importance of phase in images is particularly relevant to registration [5], [6]. The technique is outlined in [7] which indicates that the method works even when the overlapping areas of the images to be registered is small and also when the level of noise is substantial. More recent work [8],[9],and [10] indicates that the method can be used to measure misregistrations within a few percent of one pixel separation. The approach we have taken derives the registration shifts in real space rather than in frequency space and has much in common with the optical image correlators of [11],[12],and[13]. The technique can also tolerate small amounts of rotation and scaling errors. Typically a 2.5% variation in scaling causes a 60% reduction in the correlation peak. Also a  $3^\circ$  rotation typically gives the same reduction [14], [15], [16]. Although the peaks are reduced, their locations are still related to image shifts.



**FIGURE 4.**

*Grey-scale coded height map of \$ 200 coin die.*

*Note location of the three sample regions.*

*Image size: 560x560 pixels*

*Region size: 128x128 pixels*

*Grey-scale: low regions.....dark  
high regions.....light*

## DETECTION OF IMAGE SHIFT, ROTATION AND SCALING

Phase-only correlation alone can only give the x-y shift between two images. However, by breaking the images up into several regions and finding the x-y shift for each region it is possible to deduce the rotation and scaling

difference of the two images. In principle only two separate regions are needed in each image. By using three regions an indication of the data consistency can be obtained and erroneous x-y shifts detected. Figure 4 shows a typical profilometer image (of a coin die) with the three selected regions outlined in white. Note that this image represents the surface height over an array of 560x560 points (in this instance) with each region containing 128x128 points. The 8-bit height information is here grey-scale coded such that light regions are high while dark region are low. Using phase-only correlation the x-y shift for each region is calculated. Figure 5 shows the geometric parameters used for the shift, rotation, and scaling evaluation. The three arrows represent the calculated shift of each of three separate regions from the 0° image to the 180° image. Improved accuracy and reliability could be achieved by using more regions.

**Mean shift**

$$\bar{x} = (\bar{x}_1 + \bar{x}_2 + \bar{x}_3) / 3$$

$$\bar{y} = (\bar{y}_1 + \bar{y}_2 + \bar{y}_3) / 3$$

**Mean rotation angle ( $\alpha$ )**

$$\tan(\alpha) = (\bar{y}_3 - \bar{y}_1) / 2X$$

**Mean scale factor**

$$s = (2X - \bar{x}_1 + \bar{x}_3) / 2X$$

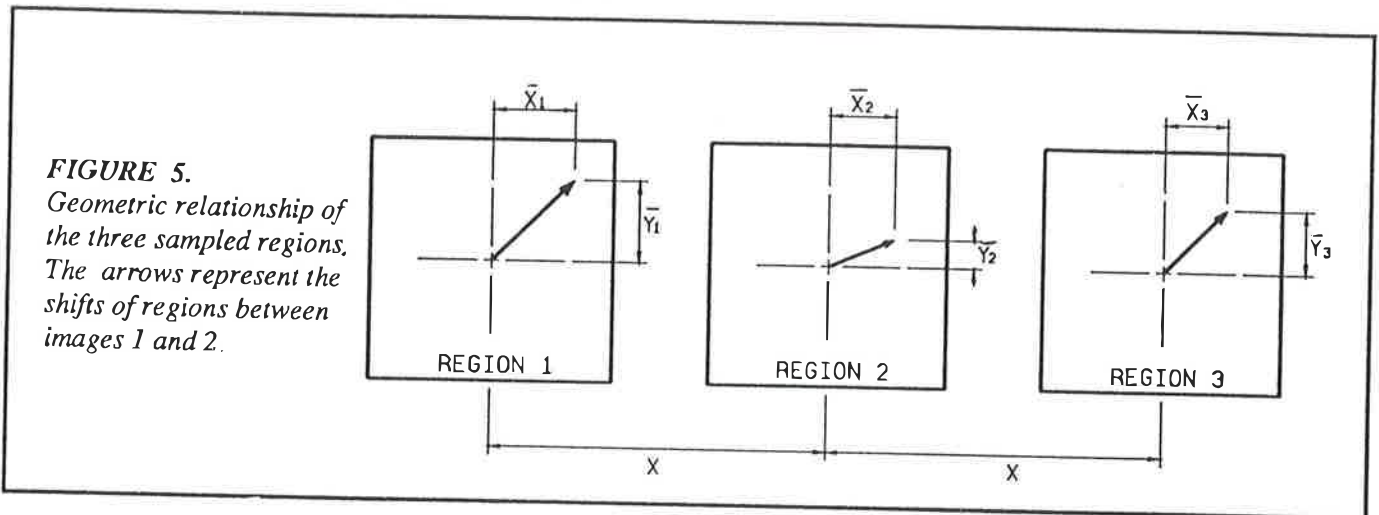
**Rotation inconsistency**

$$c_r = 2\bar{y}_2 - \bar{y}_1 - \bar{y}_3$$

**Scaling inconsistency**

$$c_s = 2\bar{x}_2 - \bar{x}_1 - \bar{x}_3$$

The last two parameters ( $c_r, c_s$ ) give an indication (in pixels) of the discrepancy in the rotation and scaling factors respectively. The inter-region separation here is X.



### PHASE-ONLY CORRELATION IMAGE REGISTRATION

The memory of the present computer system limits the phase-only correlation technique to 64x64 arrays. Initially this produced inaccurate shift values for large (>16) image shifts. The system now uses 128x128 regions which are smoothed and converted to 64x64 arrays. There is a loss in accuracy by a factor of 2, but it is still adequate. It should be mentioned that this 128 to 64 conversion can introduce significant amounts of aliasing. The effects of aliasing have been discussed in detail in [8],[9], and [10]. To reduce errors due to aliasing we use a technique in the real space domain which is closely related to the frequency space method used in [10]. The mathematical principles of phase-only correlation are easier to demonstrate for continuous functions. Modifications for discrete images and discrete transforms are straightforward but unnecessary for an overview of the technique [17], [18].

Consider an image region in image 1 represented by  $z_1 = f_1(x,y)$ , and in image 2 represented by  $z_2 = f_2(x,y)$ .

Figure 6a and 6b show 64x64 image regions corresponding to the leftmost region of figure 4 :  $f_1$  and  $f_2$ .

The following relation holds:

$$f_2(x,y) = f_1(x - x_0, y - y_0) + n(x,y) \quad (5)$$

where the image discrepancy function  $n(x,y)$  includes the effects of noise, aliasing, non-overlapping areas, rotation and scaling, and also non-overlapping shadow areas. The Fourier transform is defined as follows:

$$F(u,v) = \int_{-\infty}^{\infty} \int_{-\infty}^{\infty} f(x,y) \cdot \exp(-2\pi i[ux + vy]) \cdot dx \cdot dy \quad (6)$$

The transform/inverse transform symbol,  $\Leftrightarrow$  is defined:  $F(u,v) \Leftrightarrow f(x,y)$

Hence:  $F_1(u,v) \Leftrightarrow f_1(x,y)$

$F_2(u,v) \Leftrightarrow f_2(x,y)$

$N(u,v) \Leftrightarrow n(x,y)$

The well known Fourier shift theorem applied to  $f_2(x,y)$  gives:

$$F_2(u,v) = F_1(u,v) \cdot \exp(-2\pi i[ux_0 + vy_0]) + N(u,v) \quad (7)$$

It is more convenient to express the above transform in term of phase and modulus, hence:

$$F_1(u,v) = |F_1| \cdot \exp[i\theta_1(u,v)]$$

$$F_2(u,v) = |F_2| \cdot \exp[i\theta_2(u,v)]$$

$$N(u,v) = |N| \cdot \exp[i\psi(u,v)]$$

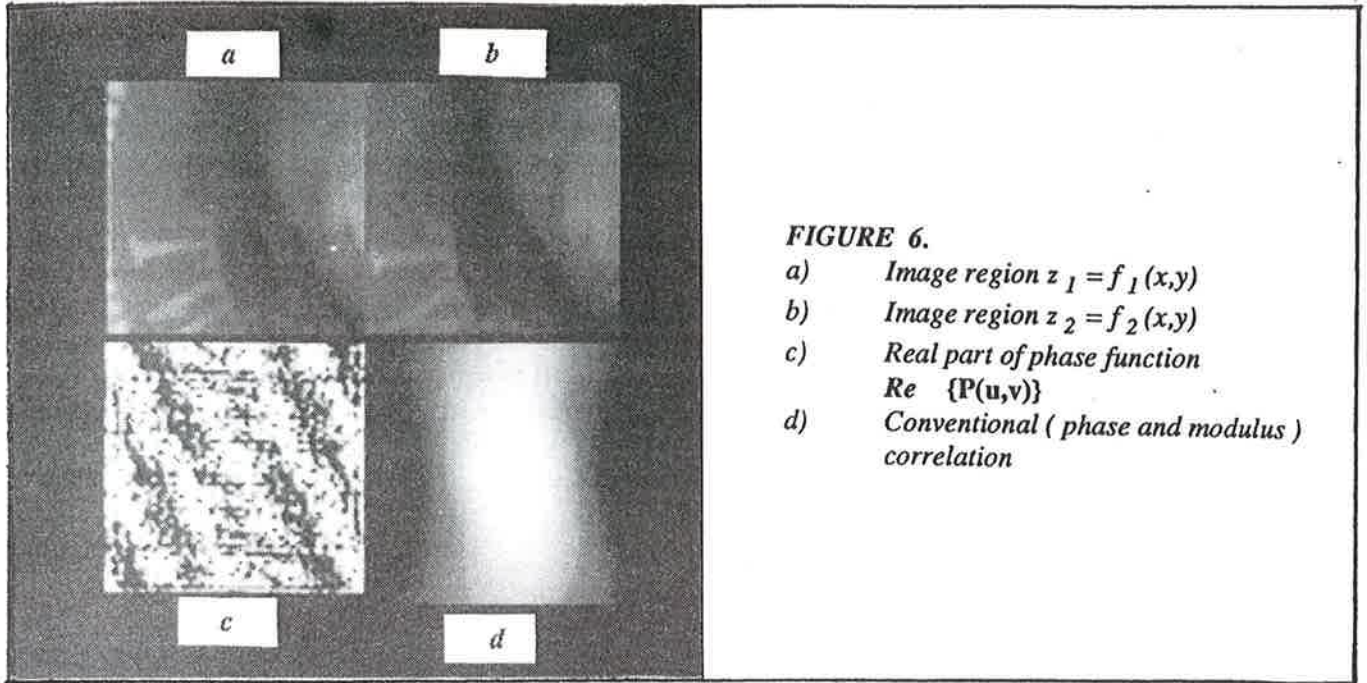


**FIGURE 6.**

- a) Image region  $z_1 = f_1(x,y)$
- b) Image region  $z_2 = f_2(x,y)$
- c) Real part of phase function  $Re \{P(u,v)\}$
- d) Conventional ( phase and modulus ) correlation

The phase-only function,  $P(u,v)$  can now be defined from the the phase difference function  $\phi$ , such that:

$$\phi(u,v) = \theta_2 - \theta_1 \quad \text{and} \quad P(u,v) = \exp[i\phi(u,v)]. \quad (8)$$

It can then be shown that:

$$P(u,v) = |R_1| \cdot \exp(-2\pi i[ux_0 + vy_0]) + |R_2| \cdot Q(u,v) \quad (9)$$

Where:  $|R_1| = |F_1| / |F_2|$

$$|R_2| = |N| / |F_2|$$

$$Q = \exp[i(\psi - \theta_1)]$$

Figure 6c shows a 64x64 image of the real part of  $P(u,v)$ . The periodic structure of  $\cos(2\pi[ux_0 + vy_0])$  is clear.

An inverse transform gives:

$$p(x,y) = r_1(x - x_0, y - y_0) + r_2(x,y) \bullet q(x,y) \quad (10)$$

where:

$$Q \Leftrightarrow q$$

$$R_1 \Leftrightarrow r_1$$

$$R_2 \Leftrightarrow r_2$$

and  $\bullet$  represents 2-D convolution.

Note  $r_1$ , and  $r_2$  are real even functions.  $q$  is a real function without any particular symmetries. Hence  $p$  is real.

Typically  $r_1(x - x_0, y - y_0)$  is a very sharp peaked function. Its centroid is located exactly at  $(x_0, y_0)$ .

Figure 6d shows a 2-D magnitude plot of the conventional (phase and modulus) correlation. Note the broad peak.

Figure 7 shows a 3-D plot of  $p(x,y)$  with corresponding shifts  $x_0=6, y_0=4$ . The peak has been normalised to 255.

Because of the 128 to 64 conversion the peak appears near location (3,2). Figure 8 shows a 3-D plot of  $p(x,y)$  with corresponding shifts  $x_0=34, y_0=20$ . Again the peak is normalised and appears this time near (17,10). In both cases the delta function is clearly visible.

The location of the main maxima of the correlation function  $p(x,y)$  is not necessarily a good indicator of the image shift when sub-pixel accuracy is required. Similarly the linear least squares fit to the phase function  $\phi(u,v)$  gives a biased estimate of the image shift if aliasing is present [8]. However if the centroid of  $p(x,y)$  is used as a measure of the shift then it can be shown that this corresponds to the gradients of the function  $\phi(u,v)$  at zero frequency. Aliasing generally disturbs the higher frequencies more than the lower ones, consequently the zero frequency gradients are less affected by aliasing.

The centroid  $(\bar{x}, \bar{y})$  is defined by:

$$\bar{x} = \frac{\int \int x \cdot p(x,y) \cdot dx \cdot dy}{\int \int p(x,y) \cdot dx \cdot dy} \quad (11)$$

And similarly for  $\bar{y}$

$$\text{Using the Fourier derivative theorem [ 17 ]: } \bar{x} = \frac{1}{(-2\pi i)} \cdot \frac{\partial P(0,0)}{\partial u} \cdot \frac{1}{P(0,0)} \quad (12)$$

$$\text{But } P(0,0) = 1 \text{ hence: } \frac{\partial P(0,0)}{\partial u} = \frac{\partial \phi(0,0)}{\partial u} \quad \text{therefore} \quad \bar{x} = \frac{1}{(-2\pi i)} \cdot \frac{\partial \phi(0,0)}{\partial u} \quad (13)$$

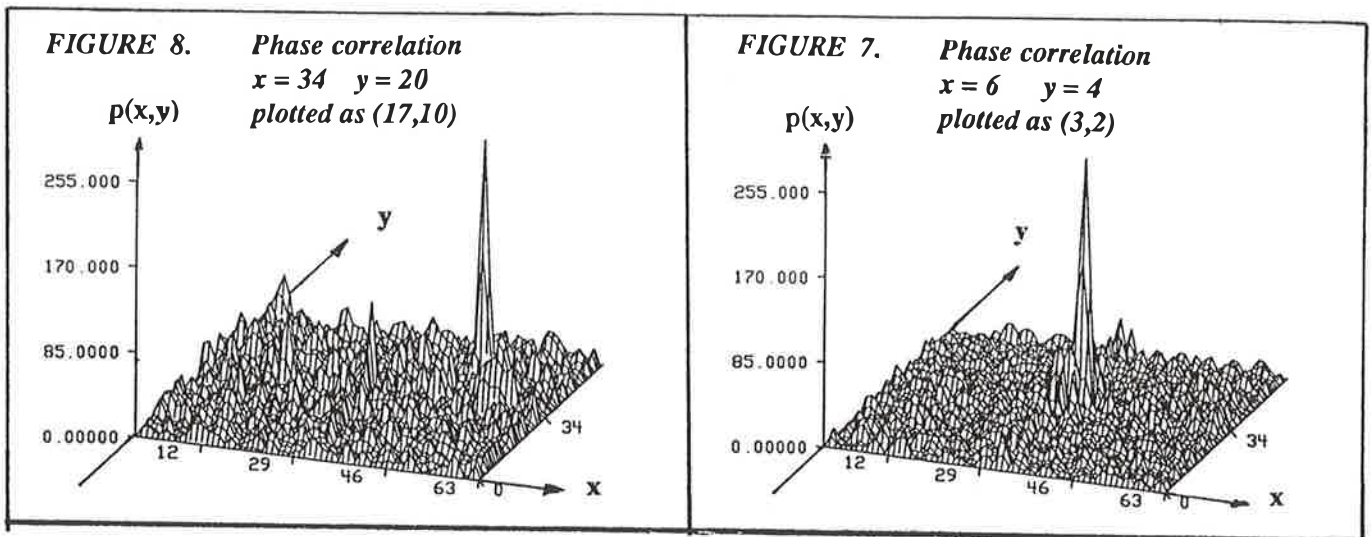
A similar relation can be derived for  $\bar{y}$ . Generally, in the discrete frequency domain of a discrete image the gradient is undefined at each pixel and a finite difference method must be used to estimate the gradient. However, in the the real space domain the corresponding centroid can be readily evaluated. Errors in the measured shift are related to the centroid of the term  $r_2(x,y) \bullet q(x,y)$  and its integrated magnitude. Several methods are available to reduce its effect. One of the most effective is to repeat the correlation cycle. On the first cycle discrepancies due to non-overlap may be significant, but the shift can still be estimated to better than one pixel. On the second cycle the non-overlapping areas are removed and the correlation used to obtain subpixel resolutions. A disadvantage is that several Fast Fourier

Transforms (FFTs) and inverse FFTs must be performed for each cycle. Another possible method is to use a window (or taper) function on the image regions to reduce the contribution of outer regions where non-overlap occurs. Finally, applying a low pass filter to  $P(u,v)$  before inverse transforming has been found empirically to improve the accuracy. This is in fact equivalent to convolving  $p(x,y)$  with a corresponding kernel. The actual implementation of this technique in the OSP uses only one cycle without tapering. Returning to Figures 7 and 8 the calculated centroid values are as follows:

Figure 7  $\bar{x} = 5.96$   $\bar{y} = 3.92$

Figure 8  $\bar{x} = 33.85$   $\bar{y} = 20.01$

In this instance the errors are all less than 0.16 pixels. Some tests have been carried out using manually shifted coin tooling, and the computed shifts compared to the x-y micrometer readings. Generally the accuracy is better than 0.3 pixels over the range  $\pm 20$  pixels. Some care has been taken in the positioning of the three sample regions (see figure 4) so that the samples do not contain large step or edge features often found at the outer rim of coin dies. These features, when present in one image region but not in the other, often give rise to spurious correlation peaks and must be avoided.



### SUMMARY OF SHADOW RESTORATION PROCESS

- A** Calculate height function for  $0^\circ$  image: Call this  $g_1(x,y)$ . Identify shadow regions.
- B** Calculate height function for  $180^\circ$  image. Call this  $g_2(x,y)$ . Identify shadow regions.
- C** Rotate second image through  $180^\circ$ . Call this  $g'_2(x,y) = g_2(-x,-y)$ .
- D** Determine x-y shift, rotation, and scaling relation of  $g_1$  and  $g'_2$ .
- E** Shift, rotate, and scale  $g'_2$  and accordingly. This results in  $g''_2(x,y)$ .
- F** Replace all shadowed data in  $g_1(x,y)$  with unshadowed data from  $g''_2(x,y)$ .

Part **D** of this process consists of the following steps:

- 1 Select suitable windows of both images. Call these samples  $f_1(x,y)$  and  $f_2(x,y)$ .
- 2 Calculate FFT of each:  $F_1(u,v)$  and  $F_2(u,v)$ .
- 3 Calculate phases of  $F_1$  and  $F_2$  Call these  $\theta_1$  and  $\theta_2$ .
- 4 Subtract phases:  $\phi = \theta_2 - \theta_1$ .
- 5 Form phase only function:  $P = \exp(i\phi)$ .
- 6 Calculate inverse FFT of  $P(u,v) \Leftrightarrow p(x,y)$ .
- 7 Convolve  $p$  with suitable kernel (or multiply  $P$  by corresponding filter before IFFT).
- 8 Locate peak position, as defined by centroid of  $p$ .
- 2 Repeat process 1 to 8 for several predetermined image regions.

### CONCLUSION

Software has been developed to restore shadow details in three dimensional measurements. The phase-only correlation technique gives an accuracy of better than 0.3 pixel over a range of  $\pm 20$  pixels for typical height distributions of coin dies. The method presented can check the consistency of the measurements and is found to be robust in the presence of missing and spurious pixel values. The correspondence of the real space centroid with the frequency space gradients has been demonstrated.

## REFERENCES

1. Srinivasan V., Liu H.C., and Haliou M., "Automated phase-measuring profilometry of 3-D diffuse objects", *Applied Optics*, Vol 23, No. 18, September 1984, pp. 3105-3108.
2. Srinivasan V., Liu H.C., and Haliou M., "Automated phase-measuring profilometry: a phase mapping approach", *Applied Optics*, Vol.24, No. 2, January 1985, pp.185-188.
3. Hariharan P., Oreb B.F., and Eiju T. "Digital phase-shifting interferometry: a simple error compensating phase calculation algorithm", *Applied Optics*, Vol26,No.13,July 1987, pp.2504-2506.
4. Tian Q., and Huhns M.N., "Algorithms for subpixel registration", *Computer Vision, Graphics, and Image Processing*, Vol.35, 1986, pp. 220-233.
5. Oppenheim A.V., Lim J.S., Kopec G., Pohlig S.C., "Phase in speech and pictures", *IEEE Int. Conf. on Acoustics, Speech, and Signal Processing*, 1979, pp. 632-637.
6. Oppenheim A.V., Lim J.S., "The Importance of Phase in Signals", *Proc. of the IEEE*, Vol. 69, No. 5, May 1981, pp.529-541.
7. Kuglin C., and Hines D., "The phase correlation image alignment method", *International Conference on Cybernetics and Society*, Proc. 1975 (IEEE), pp. 163-165.
8. Berman M., Green A.A., Bischof L., Davies S.J., and Craig M.D., "A comparison of methods for estimating band-to-band misregistrations", *Proc. Fifth Australasian Remote Sensing Conf.*, Perth, October 1990, pp. 987-996.
9. Berman M., Green A.A., Bischof L., Davies S.J., and Craig M.D., "Estimating band-to-band misregistrations in multivariate imagery", *Proc. Interface*, 1991, To appear.
10. Berman M., Bischof L., Craig M.D., Davies S.J., and Green A.A., "Estimating time delay in the presence of aliasing", Submitted to *J. Roy. Statist. Soc. B*.
11. Horner J.L., and Gianino P.D., "Phase-only Matched Filtering", *Applied Optics*, Vol.23, No.6, March 1984, pp. 812-816.
12. Dickey F.M., and Romero L.A., "Dual optimality of the phase-only filter", *Optics Letters*, Vol. 14, No. 1, January 1989, pp. 4-5.
13. Refrigier Ph., "Optimal trade-off filters for noise robustness, sharpness of the correlation peak, and Horner efficiency", *Optics Letters*, Vol. 16, No. 11, June 1991, pp. 829-831.
14. Gianino P.D., and Horner J.L., "Additional properties of the phase-only correlation filter", *Opt. Eng.*, Vol. 23, No. 6, November 1984, pp. 695-697.
15. DeCastro E., and Morandi C., "Registration of translated and rotated images using finite Fourier transforms", *IEE Trans. Pattern Anal. Machine Intell.*, Vol. 9, No. 5, September 1987, pp.700-703.
16. Vijaya Kumar B.V.K., Lee A.J., Connelly J.M., "Estimating object rotation and scale using correlation filters", *Optical Engineering*, Vol. 28, No. 5, May 1989, pp.474-481.
17. Bracewell R.N., The Fourier Transform and Its Applications , McGraw-Hill,1965
18. Brigham E.O., The Fast Fourier Transform and Its Applications , Prentice Hall, 1988